16 Apr 2004, 4:30pm - 6:30pm

Measurements and Numerical Prediction of High Speed Train Vibrations

Janusz Kogut
K. U. Leuven, Leuven, Belgium

Geert Degrande
K. U. Leuven, Leuven, Belgium

Geert Lombaert
K. U. Leuven, Leuven, Belgium

Lincy Pyl
K. U. Leuven, Leuven, Belgium

Wim Haegeman
Ghent University, Zwijnaarde, Belgium

See next page for additional authors


Proceedings: Fifth International Conference on Case Histories in Geotechnical Engineering
New York, NY, April 13-17, 2004

MEASUREMENTS AND NUMERICAL PREDICTION OF HIGH SPEED TRAIN VIBRATIONS

Janusz Kogut, Geert Degrande, Geert Lombaert, Lincy Pyl
K.U.Leuven
Kasteelpark Arenberg 40
B-3001 Leuven, Belgium

Wim Haegeman, Lutz Karl
Ghent University
Technologiepark 9
B-9052 Zwijnaarde, Belgium

ABSTRACT

This paper discusses the experimental validation of a numerical prediction model for train induced vibrations. The model fully accounts for the dynamic interaction between the train, the track and the soil. The track is modelled as a longitudinally invariant system, where two beams represent the rails, while a plate with a rigid cross section represents the subgrade. The track is located at the surface of a horizontally layered elastic halfspace. The translational invariance of the problem geometry enables a solution of the equations of motion in the frequency–wavenumber domain. The model is validated by means of vibration measurements that have been performed at the occasion of the homologation tests of the new HST track on the line L2 between Brussels and Köln during the passage of an IC train and a Thalys HST at variable speed.

INTRODUCTION

The development of the high speed train (HST) network in Europe, the USA and Asia has increased the attention for the dynamic track–soil interaction problem and railway induced vibrations.

Train induced vibrations are characterized by a number of excitation mechanisms, such as quasi–static excitation, parametric excitation, transient excitation due to rail joints and wheelflats and excitation due to wheel and rail roughness, determining the dynamic axle loads. The interaction between the train and the track cannot be disregarded, as the resonance of the axle mass or the entire vehicle against the stiffness of the track plays an important role. The dynamic interaction forces are transmitted to the soil and generate waves that propagate in the soil and may impinge on the foundations of nearby structures.

For HST tracks on soft soils, the train speed can be close to or larger than the critical phase velocity of the coupled track-soil system. In this case, the quasi–static contribution of the load is important for both the track and the free field response. High vibration levels and track displacements are obtained, affecting track stability and safety. For the X–2000 high speed train in Sweden, track deformations upto 10 mm have been reported by Adolfsson et al. (1999) at a site in Ledsgård along the West Coast Line.

The dynamic track–soil interaction problem has recently received considerable attention. Metrikine and Popp (2000) model the track as an elastic beam, supported by an elastic halfspace, formulating the equations of motion of the coupled system in the frequency–wavenumber domain. A similar formulation of the dynamic track–soil system is used by Lieb and Sudret (1998). Sheng et al. (1999a, 1999b) couple an infinite layered beam model for the track to a layered model of the soil, using Haskell–Thompson transfer matrices for the soil, considering the case of fixed and moving harmonic point sources on the track.

Within the frame of this paper, a numerical prediction model formulated in the frequency–wavenumber domain is considered (Lombaert et al. 2003). The dynamic substructure method is used to couple the track–soil system. The soil impedance is calculated by means of a boundary element method (BEM), based on the Green's functions of a horizontally layered halfspace. The model fully accounts for the dynamic interaction between the vehicle, the track and the soil by means of a compliance formulation in the frame of reference that moves with the vehicle.

In August and September 2002, the Belgian Railway company NMBS has organized homologation tests of the new HST track on the line L2 between Brussels and Köln. These tests have been performed with both an IC train and a Thalys HST and offered the unique opportunity to perform in situ vibration measurements on the track and in the free field for a wide range of train speeds between 160 and 330 km/h (Kogut et al. 2003). These data are used in the present paper for the experimental validation of the numerical prediction model.

THE NUMERICAL PREDICTION MODEL

The study of free field vibrations generated by railway traffic is a complex problem that requires the simultaneous solution of the equations of motion of the train, the track and the soil. In the following, a numerical model that fully accounts for the train–track–soil interaction is described. A method proposed by Clouteau et al. (2001) and Aubry et al. (1994) is used to study the interaction of an infinite beam with a horizontally layered elastic halfspace in the frequency-wavenumber domain. The soil's impedance is calculated by means of a boundary element method (BEM), based on the Green's functions of a horizontally, layered halfspace (Luco and Apsel 1983). The model accounts for the dynamic interaction between the train, the track and the soil by means of a compliance formulation in the frame of reference that moves with the train.

The train-track interaction problem

The dynamic axle loads applied by the train on the track are determined by the dynamic interaction between the train, the track and the soil (figure 1).

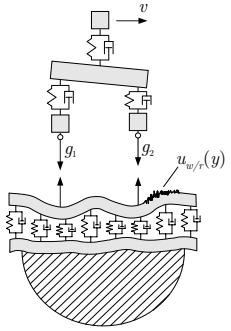

Figure 1: The train–track–soil interaction problem.

In the following, the contact between the axles and the rails is approximated by point contacts and only the vertical interaction is considered. In the fixed frame of reference, the distribution of n vertical axle loads on the coupled track-soil system is written as the summation of the product of Dirac functions that determine the time-dependent position $\{x_S, y_k + vt, z_S\}^T$ and the time history $g_k(t)$ of the k-th axle load:

$$\mathbf{F}(x,y,z,t) = \sum_{k=1}^{n} \delta(x-x_S)\delta(y-y_k-vt)\delta(z-z_S)g_k(t)\mathbf{e}_z \quad (1)$$

y_k is the initial position of the k-th axle that moves with the train speed v along the y-axis. $\mathbf{e}_z$ denotes the vertical unit base vector.

The equations of motion of the vehicle are written in the frequency domain:

$$\begin{bmatrix} \mathbf{S}_{bb} & \mathbf{S}_{ba} & 0 \\ \mathbf{S}_{ab} & \mathbf{S}_{aa}+\mathbf{S}_{aa}^W & -\mathbf{S}_{aa}^W \\ 0 & -\mathbf{S}_{aa}^W & \mathbf{S}_{aa}^W \end{bmatrix} \begin{Bmatrix} \hat{\mathbf{u}}_b \\ \hat{\mathbf{u}}_a \\ \hat{\mathbf{u}}_c \end{Bmatrix} = \begin{Bmatrix} \mathbf{0} \\ \mathbf{0} \\ -\hat{\mathbf{g}} \end{Bmatrix} \quad (2)$$

where the vectors $\hat{\mathbf{u}}_b$, $\hat{\mathbf{u}}_a$ and $\hat{\mathbf{u}}_c$ collect the displacements of the body, the axle and the contact points between the axles and the rail, respectively. Equation (2) can alternatively be written as:

$$\begin{bmatrix} \bar{\mathbf{S}}_{aa}+\mathbf{S}_{aa}^W & -\mathbf{S}_{aa}^W \\ -\mathbf{S}_{aa}^W & \mathbf{S}_{aa}^W \end{bmatrix} \begin{Bmatrix} \hat{\mathbf{u}}_a \\ \hat{\mathbf{u}}_c \end{Bmatrix} = \begin{Bmatrix} \mathbf{0} \\ -\hat{\mathbf{g}} \end{Bmatrix} \quad (3)$$

where $\bar{\mathbf{S}}_{aa} = \mathbf{S}_{aa} - \mathbf{S}_{ab}\mathbf{S}_{bb}^{-1}\mathbf{S}_{ba}$ denotes the Schur complement of the vehicle's dynamic stiffness matrix. The displacement vector $\hat{\mathbf{u}}_c$ is equal to the sum of the track (rail) displacement $\hat{\mathbf{u}}_r$ and the track (rail) unevenness $\hat{\mathbf{u}}_{w/r}$:

$$\hat{\mathbf{u}}_c = \hat{\mathbf{u}}_r + \hat{\mathbf{u}}_{w/r} \quad (4)$$

It follows immediately from equations (3) and (4) that the interaction forces can be written as:

$$\hat{\mathbf{g}} = \mathbf{S}_{aa}^W \left[\hat{\mathbf{u}}_a - \left(\hat{\mathbf{u}}_r + \hat{\mathbf{u}}_{w/r}\right)\right] \quad (5)$$

where the matrix $\mathbf{S}_{aa}^W$ denotes the dynamic stiffness matrix corresponding to the Hertzian springs between the wheels and the rails. In the case of a perfect contact between the wheels and the rails, this stiffness is infinitely large and the axle displacements $\hat{\mathbf{u}}_a$ are equal to the displacements of the contact points $\hat{\mathbf{u}}_c$, or, according to equation (4):

$$\hat{\mathbf{u}}_a = \hat{\mathbf{u}}_r + \hat{\mathbf{u}}_{w/r} \quad (6)$$

Elimination of the displacements $\hat{\mathbf{u}}_c$ of the contact points from equation (3) results into:

$$\bar{\mathbf{S}}_{aa}\hat{\mathbf{u}}_a = -\hat{\mathbf{g}} \quad (7)$$

Upon elimination of the axle displacements $\hat{\mathbf{u}}_a$ from equation (2), the following alternative equation is obtained:

$$\hat{\mathbf{u}}_c = -\hat{\mathbf{H}}^v\hat{\mathbf{g}} \quad (8)$$

where $\hat{\mathbf{H}}^v = \bar{\mathbf{S}}_{aa}^{-1} + \mathbf{S}_{aa}^{W\,-1}$ is the compliance matrix of the vehicle in the contact points between the axles and the rails. This vehicle compliance reduces to $\hat{\mathbf{H}}^v = \bar{\mathbf{S}}_{aa}^{-1}$ in the case of perfect contact between the axles and the rails.

The track displacement $\hat{\mathbf{u}}_r$ can be written in a similar way as a function of the interaction forces $\hat{\mathbf{g}}$:

$$\hat{\mathbf{u}}_r = \hat{\mathbf{H}}^t\hat{\mathbf{g}} \quad (9)$$

where each element H_{kl}^t of the track compliance matrix $\hat{\mathbf{H}}^t$ represents the Fourier transform of the track displacements at the time-dependent k-th axle position due to an impulse load at the time-dependent l-th axle position. Introduction of equations (8) and (9) into equation (4) results in the following equilibrium equation:

$$\left[\hat{\mathbf{H}}^v + \hat{\mathbf{H}}^t\right]\hat{\mathbf{g}} = -\hat{\mathbf{u}}_{w/r} \quad (10)$$

from which the interaction forces can be computed. The frequency content $\hat{\mathbf{u}}_{w/r}(\omega)$ of the track unevenness is calculated from the wavenumber domain representation $\tilde{u}_{w/r}(k_y)$ of the longitudinal unevenness profile $u_{w/r}(y)$:

$$\hat{\mathbf{u}}_{w/r}(\omega) = \frac{1}{v}\tilde{u}_{w/r}(-\frac{\omega}{v})\,\exp\left(i\omega\frac{\mathbf{y}_a}{v}\right) \quad (11)$$

where the vector $\mathbf{y}_a$ contains the initial positions y_k of all axles k.

The track–soil interaction problem

In this subsection, the equations of motion of the coupled track-soil system are solved for a vertical impulse load at a fixed track position $\{x_S, 0, z_S\}^T$. The track is assumed to be located at the surface of a horizontally layered halfspace. The invariance of the geometry with respect to y allows to perform a Fourier transformation from the longitudinal coordinate y to the horizontal wavenumber k_y. This results in a solution in the frequency–wavenumber domain, where the following equations of motion are formulated for the coupled track-soil system:

$$\left[\tilde{\mathbf{K}}_{tr} + \tilde{\mathbf{K}}_s\right]\tilde{\mathbf{u}}_{tr} = \tilde{\mathbf{f}}_{tr} \quad (12)$$

$\tilde{\mathbf{K}}_{tr}$ and $\tilde{\mathbf{K}}_s$ represent the track's and the soil's impedance, respectively, $\tilde{\mathbf{u}}_{tr}$ the track displacements and $\tilde{\mathbf{f}}_{tr}$ the forces applied to the track. For a single track as in figure 2, the track displacement vector is equal to $\tilde{\mathbf{u}}_{tr} = \{\tilde{u}_{r1}, \tilde{u}_{r2}, \tilde{u}_{sl}, \tilde{u}_{cz}\}^{\mathrm{T}}$, with $\tilde{u}_{r1}$ and $\tilde{u}_{r2}$ the vertical displacements of both rails, $\tilde{u}_{sl}$ the vertical sleeper displacement and $\tilde{u}_{cz}$ the vertical displacement at the track-soil interface Σ. The force vector is equal to $\tilde{\mathbf{f}}_{tr} = \left\{\tilde{f}_{r1}, \tilde{f}_{r2}, 0, 0\right\}^{\mathrm{T}}$. Both rails are loaded by half of a unit impulse load so that $\tilde{f}_{r1} = \tilde{f}_{r2} = 0.5$. The track impedance matrix $\tilde{\mathbf{K}}_{tr}$ can be further detailed as:

$$\tilde{\mathbf{K}}_{tr} = \begin{bmatrix} \tilde{K}_r + \tilde{K}_p & 0 & -\tilde{K}_p & 0 \\ 0 & \tilde{K}_r + \tilde{K}_p & -\tilde{K}_p & 0 \\ -\tilde{K}_p & -\tilde{K}_p & \tilde{K}_{sl} + 2\tilde{K}_p + \tilde{K}_b & -\tilde{K}_b \\ 0 & 0 & -\tilde{K}_b & \tilde{K}_b \end{bmatrix} \quad (13)$$

In the case of a classical ballasted track, the rails are modelled as Euler beams. The impedance $\tilde{K}_r = E_r I_r k_y^4 - \rho_r A_r \omega^2$ is determined by the rail bending stiffness $E_r I_r$ and the mass $\rho_r A_r$ per unit length. The railpads are modelled as continuous spring–damper connections with a dynamic stiffness defined as $\tilde{K}_p = \overline{k}_p + i\omega\overline{c}_p$. The stiffness and damping coef-

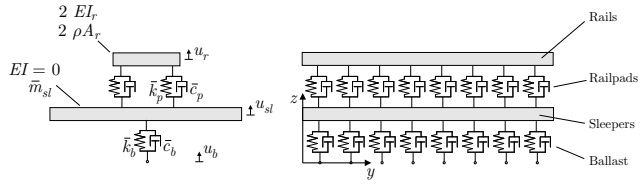

Figure 2: The track model.

ficients k_p and c_p of a single railpad are used to calculate a smeared stiffness $\overline{k}_p = k_p/d_s$ and damping $\overline{c}_p = c_p/d_s$, where d_s is the the sleeper distance. The sleepers are modelled as a continuous beam with a zero bending stiffness and a distributed mass $\rho A = \overline{m}_s = m_s/d_s$, where m_s is the sleeper mass and $\tilde{K}_{sl} = -\overline{m}_s\omega^2$. The ballast is also modelled as a continuous spring–damper connection with a dynamic stiffness $\tilde{K}_b = \overline{k}_b + i\omega\overline{c}_b$. The smeared stiffness and damping of the ballast are equal to $\overline{k}_b = 2k_b/d_s$ and $\overline{c}_b = 2c_b/d_s$, with k_b and c_b the stiffness and damping coefficients of the half of the ballast.

The soil impedance matrix $\tilde{\mathbf{K}}_s$ is equal to (Lombaert et al. 2003):

$$\tilde{\mathbf{K}}_s = \begin{bmatrix} 0 & 0 & 0 & 0 \\ 0 & 0 & 0 & 0 \\ 0 & 0 & 0 & 0 \\ 0 & 0 & 0 & \tilde{K}^s_{bb} \end{bmatrix} \quad (14)$$

where $\tilde{K}^s_{bb}$ represents the bending stiffness, which follows from the vertical equilibrium at the track-soil interface Σ and is calculated as:

$$\tilde{K}^s_{bb} = \int_\Sigma \phi_r \tilde{t}_{sz}(\tilde{\phi}_s)\, d\Gamma \quad (15)$$

$\tilde{t}_{sz}(\tilde{\phi}_s)$ is the frequency-wavenumber domain representation of $t_{sz}(\phi_s)$, the vertical component of the soil tractions $\mathbf{t}_s = \sigma_s\mathbf{n}$ on a boundary with a unit outward normal $\mathbf{n}$ for the wavefield ϕ_s scattered in the soil, while ϕ_r are the track displacement modes for each frequency and wavenumber.

A boundary element method is used to calculate the soil tractions $\tilde{t}_{sz}(\tilde{\phi}_s)$ at the track-soil interface in the soil. The boundary element formulation is based on the formulation of the boundary integral equations in the frequency-wavenumber domain, using the Green's functions of a horizontally layered soil.

The solution of equation (12) provides the soil displacement at the interface, which allows for the computation of the soil tractions $\tilde{t}_{sz}(x, k_y, z, \omega)$ at the track-soil interface Σ. The reciprocity theorem is used for the calculation of the track-soil transfer function $\tilde{h}_{zi}(\xi_1, k_y, \xi_3, \omega)$:

$$\tilde{h}_{zi}(\xi_1, k_y, \xi_3, \omega) = \int_\Sigma \tilde{u}^G_{zi}(\xi_1 - x, k_y, \xi_3, \omega)\tilde{t}_{sz}(x, k_y, z = 0, \omega)\, d\Gamma \quad (16)$$

where $\tilde{u}^G_{zi}(\xi_1, k_y, \xi_3, \omega)$ is the Green's function of the supporting horizontally layered halfspace that represents the displacement component i due to a vertical impulse load.

The response to moving loads

Accounting for the invariance of the track-soil system in the longitudinal y-direction, the Betti-Rayleigh reciprocal theorem allows to derive the following expression for the response at a point $\{\xi_x, \xi_y, \xi_z\}^T$ due to the k-th axle load in equation (1):

$$u_{si}(\xi_x, \xi_y, \xi_z, t) = \int_{-\infty}^{t} g_k(\tau) h_{zi}(\xi_x, \xi_y - y_k - v\tau, \xi_z, t - \tau)\, d\tau \quad (17)$$

The response due to a moving load on the track can therefore be calculated from the response for a concentrated impulse load at a fixed position $\{x_S, 0, z_S\}^T$ on the track.

A double forward Fourier transformation allows to derive the following expression in the frequency–wavenumber domain:

$$\tilde{u}_{si}(\xi_x, k_y, \xi_z, \omega) = \hat{g}_k(\omega - k_y v)\tilde{h}_{zi}(\xi_x, k_y, \xi_z, \omega)\exp(+ik_y y_k) \quad (18)$$

The advantage of the present equation is that the transfer function is evaluated in the frequency–wavenumber domain. Compared to the circular frequency ω observed at the receiver, a frequency shift $k_y v$ is applied to the argument of the interaction force. This shift is the cause of a phenomenon known as the Doppler effect.

The response in the space-time domain is finally obtained as the double inverse Fourier transform of equation (18).

The track compliance

In order to derive the expression for the track compliance, the transformed form of equation (18) is used to calculate the

response in a moving frame of reference $(\xi_x, \hat{\xi}_y, \xi_z, t)$, with $\hat{\xi}_y = \xi_y - vt$:

$$u_{si}(\xi_x, \hat{\xi}_y, \xi_z, t) = \frac{1}{4\pi^2} \int_{-\infty}^{+\infty} \int_{-\infty}^{+\infty} \hat{g}_k(\omega - k_y v) \hat{h}_{zi}(\xi_x, k_y, \xi_z, \omega) \exp\left[-ik_y(\hat{\xi}_y + vt - y_k)\right] \exp(+i\omega t)\, dk_y\, d\omega \quad (19)$$

The circular frequency ω is replaced by $\tilde{\omega} + k_y v$:

$$u_{si}(\xi_x, \hat{\xi}_y, \xi_z, t) = \frac{1}{2\pi} \int_{-\infty}^{+\infty} \left[\frac{1}{2\pi} \int_{-\infty}^{+\infty} \hat{g}_k(\tilde{\omega})\ \hat{h}_{zi}(\xi_x, k_y, \xi_z, \tilde{\omega} + k_y v) \exp\left[-ik_y(\hat{\xi}_y - y_k)\right]\ dk_y\right] \exp(+i\tilde{\omega} t)\, d\tilde{\omega} \quad (20)$$

The bracketed term represents the Fourier transform $\hat{u}_{si}(\xi_x, \hat{\xi}_y, \xi_z, \tilde{\omega})$ of the response in the moving frame of reference. This equation allows to derive the element $H^t_{lk}(\tilde{\omega})$ of the track compliance as:

$$H^t_{lk}(\tilde{\omega}) = \frac{1}{2\pi} \int_{-\infty}^{+\infty} \hat{h}_{zi}(\xi_x, k_y, \xi_z, \tilde{\omega} + k_y v) \exp\left[-ik_y(y_l - y_k)\right] dk_y \quad (21)$$

which represents the Fourier transform of the track response at the time–dependent position of axle l due to a unit impulse at axle k.

TRACK AND SOIL DYNAMIC CHARACTERISTICS

Dynamic characteristics of the track

The track in Lincent is a classical ballasted track. Continuously welded UIC 60 rails with a mass per unit length of $m_r = 60\,\text{kg/m}$ and a moment of inertia $I = 0.03055 \times 10^{-4}\,\text{m}^4$ are fixed with a Pandrol E2039 rail fastening system. Resilient rubber railpads of type 5197 with a thickness of 11 mm are placed under the rails, which are fixed on precast prestressed concrete monoblock sleepers with a length $l = 2.50$ m, a width $b = 0.285$ m, a height $h = 0.205$ m (under the rail) and a mass $m_s = 300$ kg. The track is supported by a porphyry ballast layer (calibre 25/50, layer thickness $d = 0.35$ m), a limestone or porphyry layer and a limestone supporting layer.

The single track model has a width of 2.5 m and is composed of two rails supported by the railpads, the sleepers and the ballast and loaded at the section's centre of gravity. The rails are modelled as continuous Euler beams.

Several vibration tests have been performed in order to determine the dynamic track characteristics. These tests include the measurement of (1) the direct and the cross receptance of the rail in a loaded and unloaded state (Kogut and Degrande 2003a), (2) the wave decay rate of the rail and (3) the transfer functions along the track.

The resonance frequency of the unloaded track on the ballast is about $f_t = 63.5$ Hz, while the rail natural frequency is around $f_r = 347$ Hz. An inverse analysis based on a periodic half track model with one rail allows to identify a dynamic stiffness of the ballast $k_b = 33$-43 kN/mm, while the damping coefficient $c_b = 45$-53 kNs/m, which is categorized as a soft-medium stiff support. The ballast is modelled as a continuous spring-damper connection between the beam and the soil, with a smeared stiffness $\overline{k}_b = 2k_b/d_s = 111.61 \times 10^6\,\text{N/m}^2$ and a damping $\overline{c}_b = 2c_b/d_s = 175.23 \times 10^3\,\text{Ns/m}^2$.

The railpad dynamic stiffness is $k_p = 102$-123 kN/mm, while the damping coefficient is $c_p = 2$-5 kNs/m, corresponding to a medium stiff railpad. In the numerical model, the railpads are a continuous spring-damper connection with a smeared stiffness $\overline{k}_p = k_p/d_s = 171.37 \times 10^6\,\text{N/m}^2$ and a smeared damping $\overline{c}_p = c_p/d_s = 7.91 \times 10^3\,\text{Ns/m}^2$.

$\rho A = \overline{m}_s = m_s/d = 500\,\text{kg/m}$ represents the sleepers mass distributed over the supporting beam.

Dynamic soil characteristics

The lithological description of the site near the HST track in Lincent reveals a layer of sandy clay with a thickness of approximately 8 m on top of a sand stratum.

Prior to the homologation tests, several complementary in situ dynamic tests have been performed to determine the soil stratification and the dynamic soil characteristics, including the Spectral Analysis of Surface Waves (SASW) test (Pyl and Degrande 2001) and the Seismic Cone Penetration Test (SCPT) (Haegeman 2001).

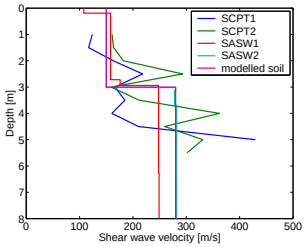

Figure 3: Measured and modelled shear wave velocity profile of the soil.

The results of the SASW and SCPT tests (figure 3) demonstrate that the site consists of a layer with a thickness of 3.0 m and a shear wave velocity of 150 m/s over a layer with a shear wave velocity of 280 m/s, which is identified as the underlying halfspace.

TRANSFER FUNCTIONS BETWEEN THE TRACK AND THE FREE FIELD

Prior to the homologation tests, the transfer functions between the track and the free field have been measured for several impacts of a falling weight on the rail head of the lower rail of track 2. A mobility function $\hat{M}_z(\omega)$ is defined as the ratio $\hat{v}_z^{\text{av}}(\omega)/\hat{F}^{\text{av}}(\omega)$ of the the average velocity $\hat{v}_z^{\text{av}}(\omega)$ and the average impact force $\hat{F}^{\text{av}}(\omega)$. Figure 4 presents the mobility at a distance of 8 m, 32 m and 64 m from the track. Superim-

posed on the same graph are the numerical results for a fixed unit impulse load at the track's centre of gravity.

The frequency content of the free field response shifts to lower frequencies with increasing distance from the source. At 8 m, the response has a broad frequency content with a maximum at about 30 Hz, while at 64 m, the maximum has shifted down to 20 Hz and the response at frequencies higher than 60 Hz is small. Results of the measurements of the transfer functions in the free field (Kogut and Degrande 2003b) are in good correspondence with the numerical results.

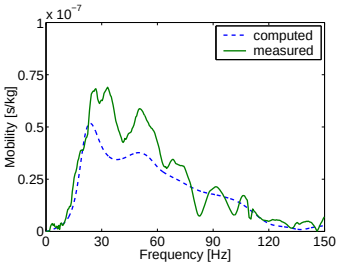

a. $\hat{v}_z(x^R = 8, \omega)$

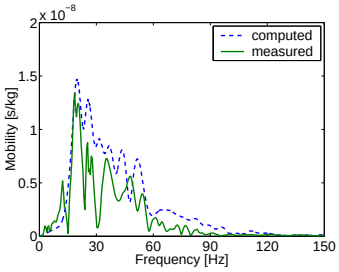

b. $\hat{v}_z(x^R = 32, \omega)$

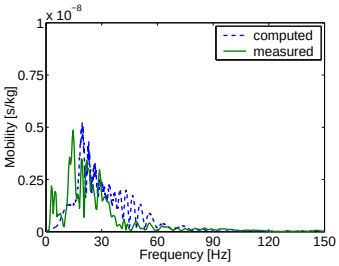

c. $\hat{v}_z(x^R = 64, \omega)$

Figure 4: The mobility measured during the impact of the falling weight and calculated with the model at 8 m, 32 m and 64 m.

THE HOMOLOGATION TESTS

Two types of trains are used during the homologation tests: an IC train and the Thalys high speed train. Figure 5 shows the Thalys HST consisting of 2 locomotives and 8 coaches. Each locomotive is supported by two bogies and has four axles. The coaches next to the locomotives have one independent bogie and share the second bogie with the neighbouring coach. The six remaining coaches share both bogies with neighbouring coaches, resulting in an articulated train composition. The total number of bogies equals 13 and, consequently, the number of axles on the train is equal to 26. The geometrical and mass

Figure 5: The Thalys HST at the site of Lincent.

characteristics of the Thalys HST are summarized in table 1.

During the homologation tests in Lincent measurements have been performed in 16 measuring points on both tracks and in a free field. The actual speed of the IC train is between 155.9 and 225.3 km/h. For the Thalys HST, the recorded speed is between 218.1 and 326.1 km/h.

A single passage of the Thalys HST

The time history and the frequency content of the velocity of the sleeper during the passage of the Thalys HST on track 2 with a speed $v = 294$ km/h are shown in figure 6. The time

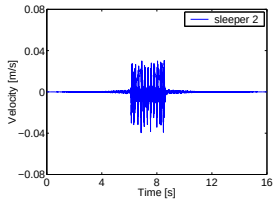

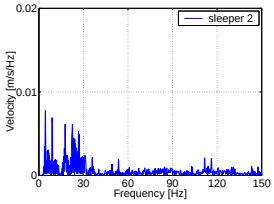

a. $v_z(Sleeper, t)$. *b.* $\hat{v}_z(Sleeper, \omega)$.

Figure 6: Time history and frequency content of the vertical velocity of the sleeper during the passage of the Thalys HST on track 2 with a speed $v = 294$ km/h.

history (figure 6a) clearly allows to identify the passage of every axle on the sleeper. The response of the track for every single axle of the train is nearly uniform. The acceleration has a quasi-discrete spectrum (figure 6b) with peaks at the fundamental bogie passage frequency $f_b = v/L_b = 4.37$ Hz ($L_b = 18.7$ m) and its higher harmonics, modulated at the axle passage frequency $f_a = v/L_a = 27.22$ Hz ($L_a = 3.0$ m).

The time history and the frequency content of the vertical velocity in the free field are shown in figure 7. At $x^R = 8$ m from the track, the peak particle velocity (PPV) is equal to 1.75 mm/s. At $x^R = 32$ m and $x^R = 64$ m from the track, the PPV is equal to 0.16 mm/s and 0.06 mm/s, respectively. Higher frequencies between 55 and 65 Hz, which are due to the train and track characteristics, are dominant in the frequency content at $x^R = 8$ m. The sleeper passage frequency is equal to $f_s = v/d_s = 136.1$ Hz. Lower frequencies are better distinguished at $x^R = 32$ m from the track. In the far field the dominant frequencies are between 20 and 30 Hz.

Table 1: Geometrical and mass characteristics of the Thalys HST.

	Number of carriages	Number of axles	L_t [m]	L_b [m]	L_a [m]	M_t [kg]	M_s [kg]	M_u [kg]
Locomotive	2	4	22.15	14.00	3.00	17000	14937	2027
Side coach	2	3	21.84	18.70	3.00	17000	14937	2027
Central coach	6	2	18.70	18.70	3.00	17000	14937	2027

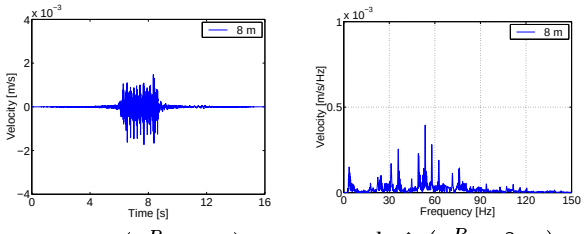

a. $v_z(x^R = 8, t)$ *b.* $\hat{v}_z(x^R = 8, \omega)$

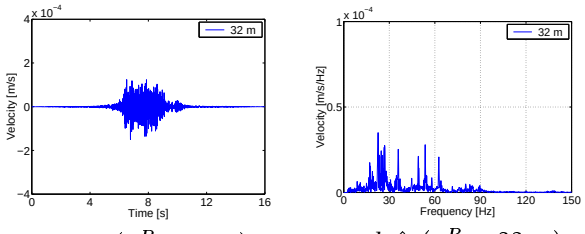

c. $v_z(x^R = 32, t)$ *d.* $\hat{v}_z(x^R = 32, \omega)$

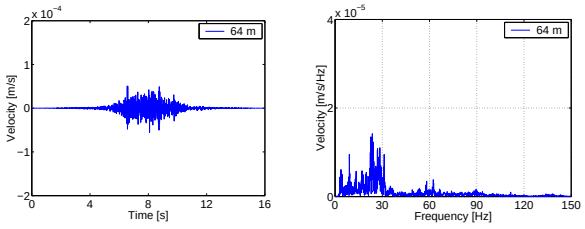

c. $v_z(x^R = 64, t)$ *d.* $\hat{v}_z(x^R = 64, \omega)$

Figure 7: Time history (left) and frequency content (right) of the free field vertical velocity at 8 m, 32 m and 64 m from the track, during the passage of the Thalys HST on track 2 with a speed $v = 294$ km/h.

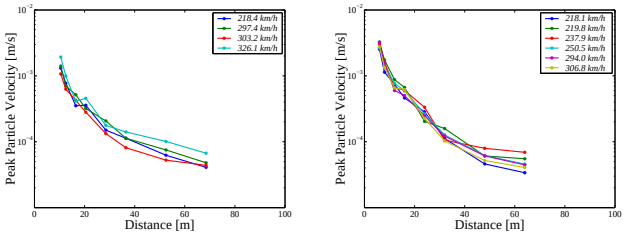

a. Track 1. *b. Track 2.*

Figure 8: Vertical PPV as a function of the distance to the track for all passages of the Thalys HST.

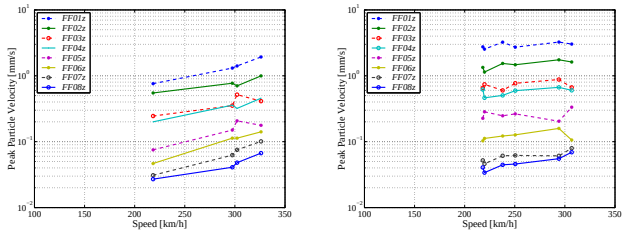

a. Track 1. *b. Track 2.*

Figure 9: Vertical PPV as a function of the train speed for all passages of the Thalys HST.

Peak particle velocity for all the passages of the Thalys HST

Figure 8 shows the vertical PPV as a function of the distance to the track for all passages of the Thalys HST on tracks 1 and 2. The distance between track 1 and the measurement points in the free field is 4.50 m larger than for track 2. The maximum value of the vertical PPV is about 3.3 mm/s at x^R = 6 m from the track. The dependence of the PPV on the train speed appears to be generally low. Comparison of the results from both tracks shows the amplitude attenuation with the distance from the track due to the material and radiation damping in the soil.

Results can better be appreciated if the PPV is shown as a function of the train speed. Figure 9 shows the PPV as a function of the train speed for all passages of the Thalys HST on tracks 1 and 2, respectively. As mentioned before, the dependence of the PPV on the train speed is moderate to low in the range of train speeds considered. Figure 9a demonstrates that the PPV in nearly all channels is slightly increasing for an increasing speed of the Thalys HST running on track 1, as is theoretically expected in the subcritical range of train speeds.

RESULTS OF THE NUMERICAL MODEL

Track unevenness

Shortly before the homologation tests, the Belgian Railway Company NMBS has used an EM-130 vehicle in order to measure the initial track unevenness. The measurements have been performed on each rail of both tracks. Figure 10 presents the Fourier transformation of the averaged unevenness of both rails on track 2 (profile `A`).

As the transfer function of the EM130 between the measured and actual unevenness is not equal to 1 in the entire wavelength range of interest, an artificial profile has been computed for the prediction of the railway vibrations. The artificial profile is derived from a power spectral density (PSD), that has been fit to the PSD of the measured profile. Figure 10 also presents the Fourier transformation of the artificial track unevenness used (profile `B`).

Train-track interaction forces

The train is modelled as a system with 26 degrees of freedom (DOF), where each DOF represents the displacement of the unsprung axle mass M_u as described in table 1.

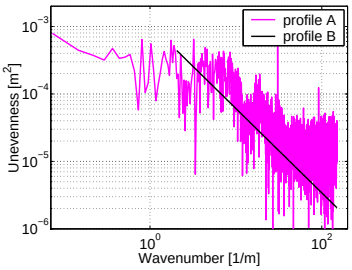

Figure 10: The Fourier spectra of an unevenness profile measured on both rails of track 2 (profile A) and an artificially generated profile B.

The interaction forces between the train and the track have been computed using the aforementioned unevenness profiles. The interaction forces are computed for the passage of the Thalys HST with a speed of 294 km/h.

Figure 11 presents the frequency content of the interaction force at the first axle computed for two unevenness profiles – profile A and profile B as shown in figure 10. The frequency content in the lower frequency range of interaction forces is dominated by frequencies between 25 and 40 Hz.

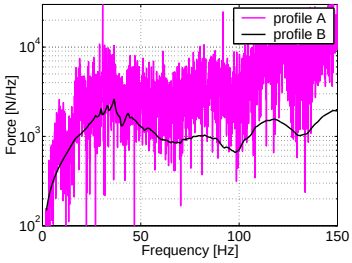

Figure 11: The train–track interaction force for the passage of the Thalys HST with a speed of 294 km/h computed for the measured (A) and generated B unevenness profiles.

The Thalys HST passage with a speed v = 294 km/h

Figure 12 presents the time history and the frequency content of the vertical velocity computed for the passage of the Thalys HST passage with a speed v = 294 km/h at a distance of 8 m, 32 m and 64 m perpendicular to the track using different unevenness profiles. The free field response has been calculated with the same track and soil parameters as for a fixed unit impulse load (figure 4).

The time history shows the uniform passage of the axles of the train in the near field at $x^R = 8$ m. The amplitude of the response is decreasing with increasing distance from the track.

Figure 12 clearly shows the wide range of dominant frequencies at a distance of 8 m from the track. When the distance from the track increases, the frequencies higher than 60 Hz are attenuated by the material and radiation damping in the soil and the frequency range between 20 and 40 Hz becomes dominant. The frequency content in all the points is very similar to the measured one, while the amplitude at the points in the far field is overestimated.

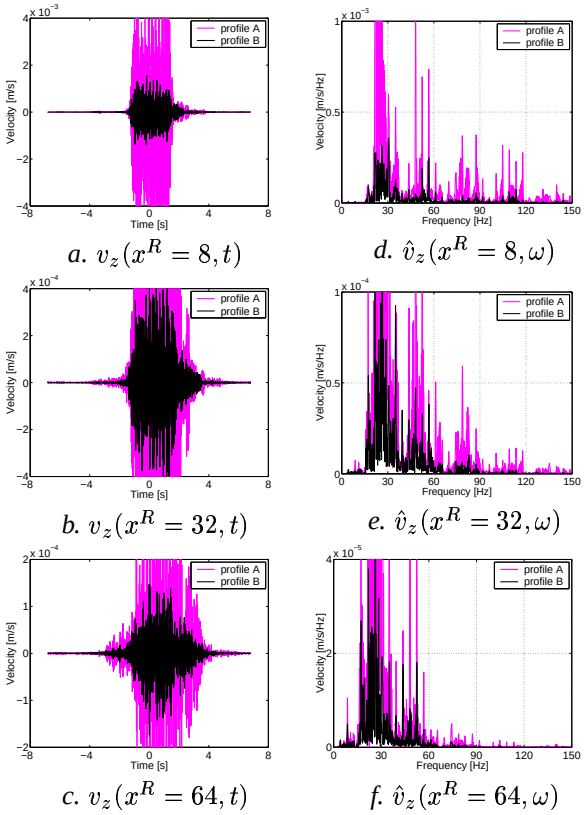

Figure 12: Time history and frequency content of the vertical velocity during the passage of the Thalys HST passage with a speed v = 294 km/h calculated with the model at 8 m, 32 m and 64 m from the track for different unevenness profiles.

Good agreement with the experimental results (figure 7) is obtained using the model with unevenness profile B as demonstrated in figure 13.

CONCLUSION

In this paper, a numerical model for the prediction of railway induced vibrations has been presented. The track is assumed to be invariant in the longitudinal direction and to be located at the surface of a horizontally layered elastic halfspace. The model fully accounts for the dynamic interaction between the train, the track and the soil by means of a compliance formulation in the frame of reference that moves with the train.

An elaborate measurement campaign has been performed to validate the numerical model. These include the results of free field surface vibration measurements during the passage of an IC and a Thalys HST train, that have been performed on the site in Lincent during the homologation tests of line L2 of the HST track between Brussels and Köln.

The results of the validation of the model have been shown for the transfer functions between the track and the soil, as well as for the free field vibrations during the passage of a Thalys HST running with a speed of 294 km/h.

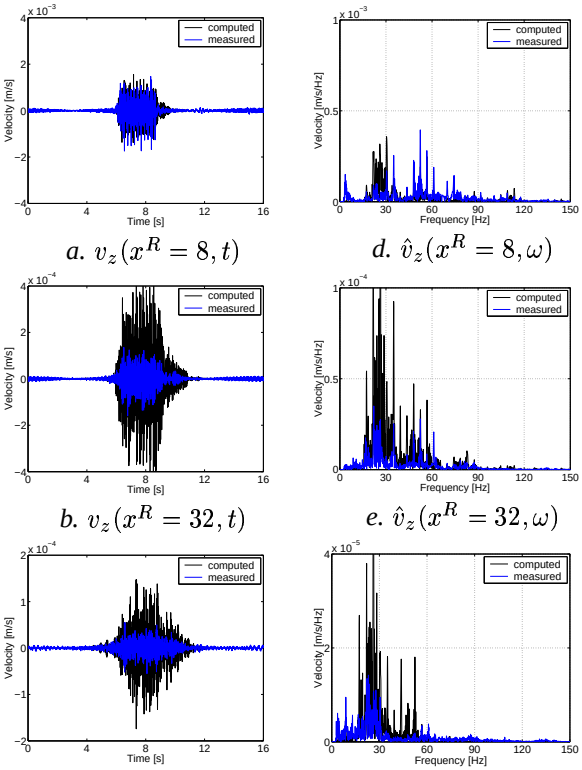

a. $v_z(x^R = 8, t)$ *d.* $\hat{v}_z(x^R = 8, \omega)$

b. $v_z(x^R = 32, t)$ *e.* $\hat{v}_z(x^R = 32, \omega)$

c. $v_z(x^R = 64, t)$ *f.* $\hat{v}_z(x^R = 64, \omega)$

Figure 13: Time history and frequency content of the vertical velocity during the passage of the Thalys HST passage with a speed v = 294 km/h at 8 m, 32 m and 64 m from the track computed using unevenness profile B and measured.

ACKNOWLEDGEMENTS

The results presented in this paper have been obtained within the frame of the STWW project IWT 000152 "Traffic induced vibrations in buildings". The financial support of the Flemish Community is kindly acknowledged.

The in situ vibration measurements have been performed in collaboration with NMBS, Technum, TNO Delft and Pandrol Rail Fastenings Limited.

REFERENCES

Adolfsson, K., B. Andréasson, P.-E. Bengtson, A. Bodare, C. Madshus, R. Massarch, G. Wallmark, and P. Zackrisson (1999). High speed lines on soft ground. Evaluation and analyses of measurements from the West Coast Line. Technical report, Banverket, Sweden.

Aubry, D., D. Clouteau, and G. Bonnet (1994, December). Modelling of wave propagation due to fixed or mobile dynamic sources. In N. Chouw and G. Schmid (Eds.), *Workshop Wave '94, Wave propagation and Reduction of Vibrations*, Rühr University, Bochum, Germany, pp. 109–121.

Clouteau, D., G. Degrande, and G. Lombaert (2001). Numerical modelling of traffic induced vibrations. *Meccanica 36*(4), 401–420.

Haegeman, W. (2001, September). In situ tests Retie-Waremme-Lincent. Report RUG IV.1.16.3, Soil Mechanics Laboratory, Ghent University. STWW Programme Technology and Economy, Project IWT-000152.

Kogut, J. and G. Degrande (2003a, March). Assessment of the dynamic parameters of the HST track L2 Brussels - Köln in Lincent using rail receptance measurements. Report BWM-2003-05, Department of Civil Engineering, Katholieke Universiteit Leuven. STWW Programme Technology and Economy, Project IWT-000152.

Kogut, J. and G. Degrande (2003b, January). Transfer functions between the HST track and the free field on the line L2 Brussels-Köln in Lincent. Report BWM-2003-03, Department of Civil Engineering, Katholieke Universiteit Leuven. STWW Programme Technology and Economy, Project IWT-000152.

Kogut, J., G. Degrande, and W. Haegeman (2003, May). Free field vibrations due to the passage of an IC train and a Thalys HST on the high speed track L2 Brussels-Köln. In *6th National Congress on Theoretical and Applied Mechanics*, Ghent, Belgium.

Lieb, M. and B. Sudret (1998). A fast algorithm for soil dynamics calculations by wavelet decomposition. *Archive of Applied Mechanics 68*, 147–157.

Lombaert, G., S. François, G. Degrande, and J. Kogut (2003, May). Validation of a numerical model for railway induced vibrations. In *6th National Congress on Theoretical and Applied Mechanics*, Ghent, Belgium.

Luco, J. and R. Apsel (1983). On the Green's functions for a layered half-space. Part I. *Bulletin of the Seismological Society of America 4*, 909–929.

Metrikine, A. and K. Popp (2000). Steady-state vibrations of an elastic beam on a visco-elastic layer under moving load. *Archive of Applied Mechanics 70*, 399–408.

Pyl, L. and G. Degrande (2001, August). Determination of the dynamic soil characteristics with the SASW method at a site in Lincent. Report BWM-2001-02, Department of Civil Engineering, Katholieke Universiteit Leuven. STWW Programme Technology and Economy, Project IWT-000152.

Sheng, X., C. Jones, and M. Petyt (1999a). Ground vibration generated by a harmonic load acting on a railway track. *Journal of Sound and Vibration 225*(1), 3–28.

Sheng, X., C. Jones, and M. Petyt (1999b). Ground vibration generated by a load moving along a railway track. *Journal of Sound and Vibration 228*(1), 129–156.